Infrared Physics and Technology 102 (2019) 102982

Contents lists available at ScienceDirect

Infrared Physics & Technology

journal homepage: www.elsevier.com/locate/infrared

Regular article

Observation of the dispersion effect of SnS_2 nanosheets in all-normal-dispersion Yb-doped mode-locked fiber laser

Jinjuan Gao[a], Jie Pan[a], Yanjun Liu[b], Quanxin Guo[a], Xile Han[a], Xinxin Shang[a], Linguang Guo[a], Zitan Zuo[a], Baoyuan Man[a], Huanian Zhang[a], Shouzhen Jiang[a,*]

[a] Shandong Provincial Key Laboratory of Optics and Photonic Device, School of Physics and Electronics, Shandong Normal University, Jinan 250014, China
[b] Department of Electrical and Electronic Engineering, Southern University of Science and Technology, Shenzhen 518055, China

ARTICLE INFO

Keywords:
SnS_2
Dispersion
All-normal-dispersion
Mode-locked
Fiber laser

ABSTRACT

In the present study, the dispersion effect of SnS_2 nanosheets was investigated by comparing two groups of data that produced by all-normal-dispersion Yb-doped mode-locked fiber laser with SnS_2 nanosheets or not. Besides, the nonlinear saturable absorption characteristics of the SnS_2 were investigated experimentally. The saturation intensity and modulation depth were 6.01 MW/cm^2 and 8.68%, respectively. The dispersion effect of SnS_2 nanosheets significantly decreased pulse width. The pulse duration was shortened to one half or one third of the original. When the pump power was 193.3 mW, the narrowest pulse width was 1.05 ns. In this study, the dispersion effect of SAs was first observed and experimentally investigated in an all-normal-dispersion laser cavity. Based on the results here, a new method can be developed to investigate passively mode-locked fiber laser and promote the practical applications of SAs in the field of ultrafast photonics.

1. Introduction

In recent years, mode-locked fiber lasers have aroused huge attention for their useful practicability in many areas, e.g. optical communication, micromachining, metrology and military systems [1–4]. Passively mode-locked fiber lasers have been extensively investigated for many of their advantages, e.g. compact structure, low cost, simplicity and the flexibility of their design [5–7]. Thus far, various types of saturable absorbers (SAs), e.g. semiconductor saturable absorption mirror (SESAM) [8,9], graphene [10–14], carbon nanotubes [15–18], topological insulators [19–25], transition metal dichalcogenides (TMDs) [26–36], and black phosphorus [37–40], have been adopted to achieve passive mode-locked lasers. For instance, Guo et al. demonstrated a sub-200 fs soliton mode-locked erbium-doped fiber laser (EDFL) using a microfiber-based bismuthene saturable absorber [40]. Bi_2Se_3 was successfully used for demonstrating a large-energy passively Q-switched erbium-doped fiber laser in 2019 [25]. Moreover, various TMDs, with the advantages of ultrafast recovery time, unusual electronic, structural properties and wide absorption, have been broadly used to achieve mode-locked or Q-switched fiber laser. Recently, IV-VI group TMDs, covering ReS_2 and SnS_2, have also aroused considerable interest. For instance, Mao et al. reported a ReS_2-polyvinyl alcohol (PVA) film based passively Q-switched and mode-locked erbium-doped fiber lasers [41]. Niu et al. have investigated the nonlinear absorption property of SnS_2 and achieved a passively Q-switched Er-doped fiber laser with minimum pulse width of 510 ns [42]. Besides, SnS_2-PVA film was successfully prepared and employed as a mode-locker in obtaining an Er-doped modelocked laser with a pulse width of 623 fs in 2018 [43].

The saturation absorption characteristics of above materials were experimentally and theoretically verified. Except the saturation absorption characteristics of materials, the characteristics of the laser system can be affected by dispersion, linear gain and loss, spectral filtering and nonlinear effect. Some researches studied special mode-locked laser phenomena by adjusting dispersion in laser system. Lin et al. experimentally investigated the bound states of multiple dispersion-managed solitons (DMSs) from a net-normal-dispersion passive mode-locked Yb-doped fiber laser [44]. Cheng et al. achieved dissipative soliton resonance in an all-normal-dispersion mode-locked Yb-doped fiber laser [45]. Nevertheless, the dispersion effect of SAs in fiber laser system has not been investigated. Accordingly, this study first investigated the dispersion effect of SAs in an all-normal-dispersion passively mode-locked ytterbium-doped fiber laser at 1064 nm. Moreover, tin disulfide (SnS_2) was used to study its dispersion effect for laser system. SnS_2 was an n-type direct bandgap semiconductor with a value of 2.24 eV. It exhibits a CdI_2 crystal structure with the sandwich structure, which is composed by two layers of close-packed sulfur

* Corresponding author.
E-mail address: jiang_sz@126.com (S. Jiang).

https://doi.org/10.1016/j.infrared.2019.102982
Received 19 April 2019; Received in revised form 9 June 2019; Accepted 16 July 2019
Available online 17 July 2019
1350-4495/

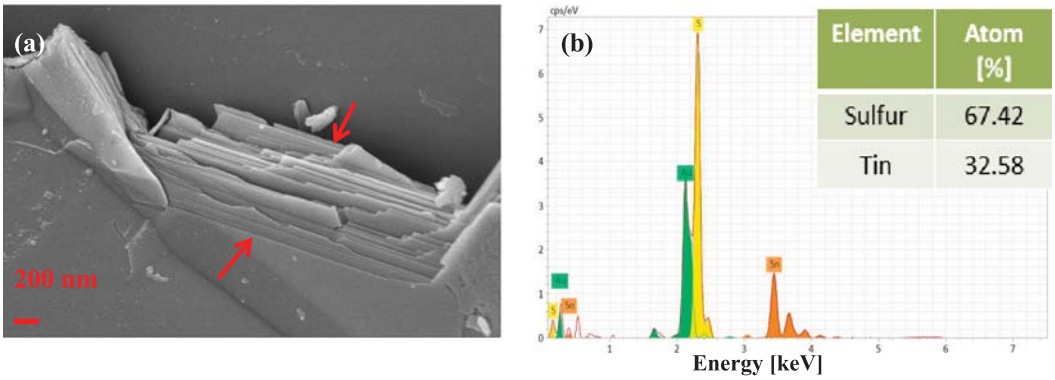

Fig. 1. (a) The SEM image of the SnS_2 nanosheets. (b) EDX spectroscopy of the SnS_2 nanosheets, inset: the atomic ratio of sulfur and tin.

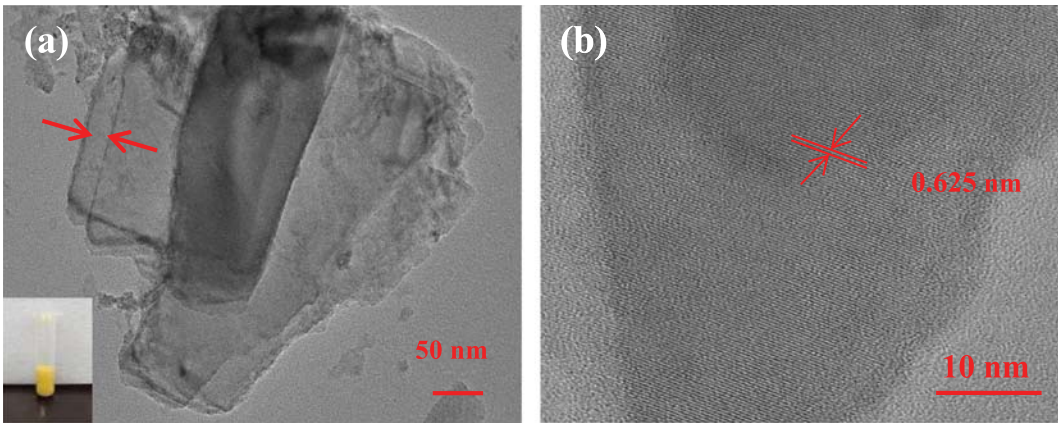

Fig. 2. (a) The TEM image of the SnS_2 nanosheets. (b) The HTEM image of the SnS_2 nanosheets. Inset of (a) The SnS_2 dispersion solution.

anions and one-layer tin cations [46–49]. Besides, the advantages of SnS_2 are low-cost, environmentally friendly and Earth-abundant, which made it better to fulfill scientific and industrial requirements.

For the first time, this study investigated the dispersion characteristics of the SnS_2 nanosheets in an all-normal-dispersion passively mode-locked Yb-doped fiber laser by contrasting the data that were produced by the all-normal-dispersion Yb-doped fiber laser with SnS_2 nanosheets or not. Besides, the nonlinear saturable absorption characteristics of the SnS_2 were investigated experimentally. The saturation intensity and modulation depth were about 6.01 MW/cm^2 and 8.68%, respectively. This study found that the dispersion effect of SnS_2 nanosheets significantly decreases pulse width. The pulse duration was shortened to one half or one third of the original. The narrowest pulse width was 1.05 ns under the pump power of 193.3 mW. Based on these results, a new method can be developed to investigate mode-locked fiber laser, which will promote the practical applications of SAs in the field of ultrafast photonics.

2. Preparation and characterization of materials

The preparation process of the SA is to be described as follow steps. Adding 1 g SnS_2 nanosheets into 100 mL alcohol (30%) is the first step to prepare a SnS_2 dispersion solution. To fully mix the SnS_2 dispersion solution still need to be placed in the ultrasonic cleaner for 12 h. Second, 5 wt% PVA solution and the SnS_2 dispersion solution were mixed at the volume ratio of 3:2. The SnS_2-PVA dispersion solution was produced by cleaning mixture dispersion solution using the ultrasonic cleaner for 4 h. Third, 180 μL SnS_2-PVA dispersion solution was spin-coated on a sapphire substrate to format the SnS_2-PVA film. Finally, a 1 × 1 mm^2 thin film was cut off and put on the end face of the photonic crystal (PC) fiber head as SAs.

The structure of SnS_2 nanosheets was analyzed by using following characterizations. The surface topography of the SnS_2 nanosheets was observed and analyzed under a scanning electron microscope (SEM). As shown in Fig. 1(a), SEM image shows that SnS_2 nanosheets have a layered structure with a resolution of 200 nm. The elemental composition and stoichiometry of the SnS_2 nanosheets were analyzed using the energy dispersion X-ray (EDX). The corresponding peaks associated with sulfur and tin are observed clearly shown in Fig. 1(b). The inset of Fig. 1(b) suggests the atomic ratio of sulfur (67.42%) and tin (32.58%) was estimated to be 2:1.

A JEM-2100 microscope with an optical resolution of 50 nm was used to record the transmission electron microscope (TEM) image of the SnS_2 nanosheets dispersion solution. SnS_2 exhibits layered structure, as clearly shown in Fig. 2(a). The inset of Fig. 2(a) suggests that SnS_2 dispersion solution is uniform yellow[1] dispersion solution. Subsequently, high crystallinity of this SnS_2 dispersion solution could be demonstrated by the regular diffraction fringes (HRTEM, Fig. 2(b)), with the lattice spacing of 0.625 nm.

Furthermore, the structure characterizations of the SnS_2 nanosheets were also investigated using the X-ray diffraction (XRD) technology and the Raman spectrum [50]. As shown in Fig. 3(a), the peaks were recorded, corresponding to the (0 0 1), (1 0 0), (0 0 2), (1 0 1), (1 0 2) and (0 0 3) planes in SnS_2. The high diffraction peaks at (0 0 1) plane in the XRD pattern is obvious, which reveals that the SnS_2 nanosheets prepared exhibit well-layered structure and high crystallinity [43]. Two Raman shift peaks can be observed in Fig. 3(b), corresponding to the A_{1g} and E_g symmetry intralayer mode at 313.04 and 203.79 cm^{-1}, which is consistent with the previously reported results [49].

The thickness characteristics of the prepared SnS_2 nanosheets were measured with an atomic force microscope (Bruker Multimode 8). In Fig. 4(a), four areas were used to analyze the height of SnS_2 nanosheets

[1] For interpretation of color in Fig. 2, the reader is referred to the web version of this article.

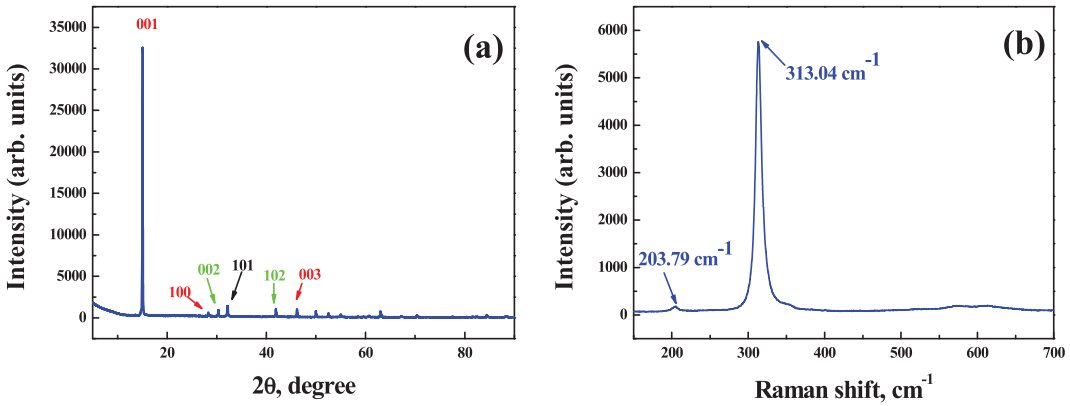

Fig. 3. (a) X-ray diffraction of the SnS_2 nanosheets. (b) Raman spectrum of the SnS_2 nanosheets.

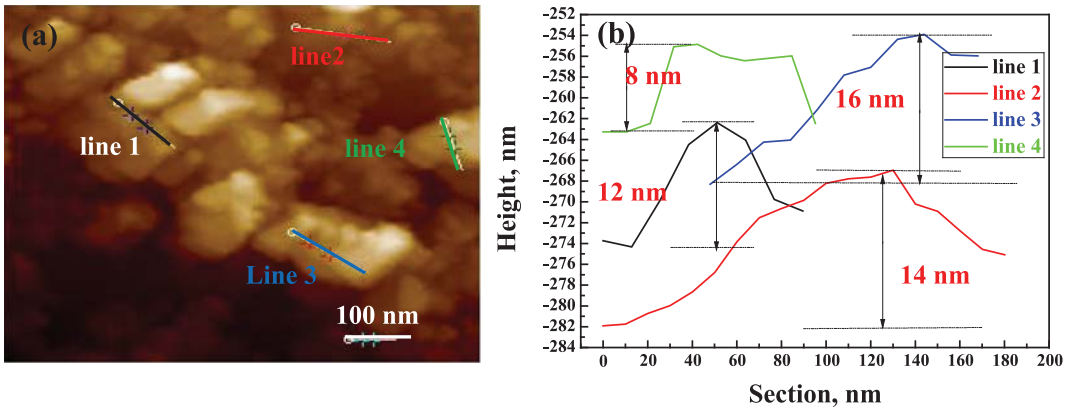

Fig. 4. (a) The AFM image of the SnS_2 nanosheets. (b) The height measurement of the selected-area in Fig. 4(a).

under the resolution of 100 nm. The thickness of these areas were measured as 8, 12, 14 and 16 nm, respectively, as shown in Fig. 4(b). Based on a predicted monolayer thickness of ≈0.6 nm [51], the layer number of the SnS_2 nanosheets in the experiment was estimated at nearly 13–26.

Using a power-dependent transmission technique, the nonlinear absorption property of the SnS_2-PVA film-type SA was investigated [52]. The experimental results are shown in Fig. 5(a). Besides, the data were fitted to the following equation [30]:

$$T(I) = 1 - T_{ns} - \Delta T \times \exp(-I/I_{sat})$$

where T denotes transmission, T_{ns} is non-saturable absorbance, ΔT is modulation depth, I is input intensity of laser, and I_{sat} is saturation intensity. The intensity and modulation depth were obtained as 6.01 MW/cm^2 and 8.68%, respectively, by fitting the experimental results. In Fig. 5(b), a UV/Vis/NIR spectrophotometer (Hitachi U-4100) was used to investigate the transmittance of the SnS_2-PVA film and the substrate versus optical wavelength. It can be clearly observed that the transmission increases with the wavelength. Moreover, the transmission of the SnS_2-PVA film at the wavelength of 1027 nm was about 73.46%.

3. Experimental details

The experimental setup of the SnS_2 nanosheets in all-normal-dispersion Yb-doped mode-locked fiber laser is shown in Fig. 6. A piece of 0.3 m Yb-doped fiber (LIEKKI Yb1200-4/125) as the laser gain medium with group velocity dispersion (GVD) of 24.22 ps^2/km was pumped

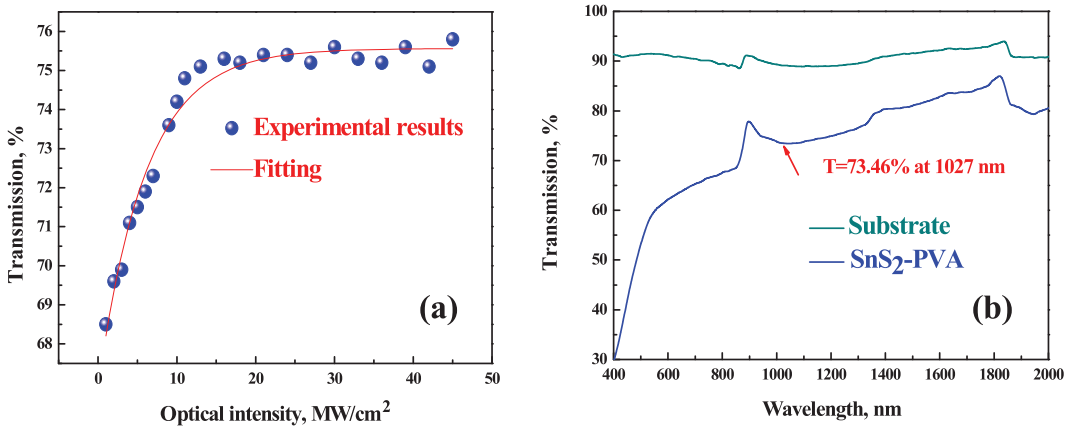

Fig. 5. (a) Nonlinear absorption property of the SnS_2-PVA film. (b) Linear transmission of the SnS_2-PVA film versus wavelength.

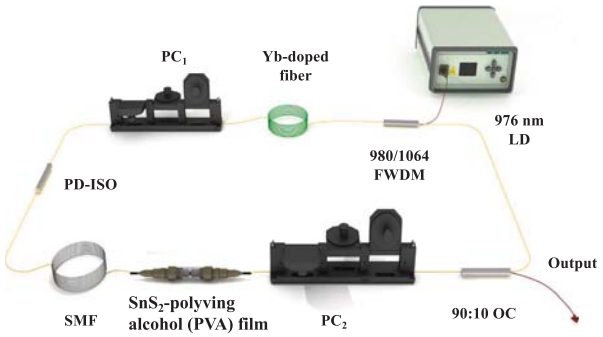

Fig. 6. Experimental setup of the noise-like mode-locked fiber laser.

using 976 nm laser diode (LD) with a 980/1064 nm filter wavelength division multiplexer (FWDM). Two polarization controllers (PCs) were used to adjust the polarization state in the cavity. A polarization-dependent isolator (PD-ISO) was used to transform the common light into linearly polarized lights, which demonstrates the mode-locked pulse output. A piece of 303.08 m long single-mode fiber (SMF-28) with GVD of 17.7 ps^2/km was adopted to increase the Kerr nonlinearity and adjust dispersion in cavity. The laser output beam was extracted through the 10% output port of a 10:90 output optical coupler (OC). The total cavity length was up to 303.38 m, suggesting that the net dispersion of the Yb-doped fiber laser was estimated at nearly 5.37 ps^2. The output performances of the fiber laser were recorded using a fast-speed photodetector (3G), a digital oscilloscope (DPO4054), a power meter (PM100DS122C), an optical spectrum analyzer (AQ6317) and a spectrum analyzer (R&S FPC1000).

4. Experimental results

Fig. 7(a) shows the output power and the pulse duration as a function of pump power in a mode-locked fiber laser without SA, only including PD-ISO and SMF. When the pump power increased from 44.5 to 226.4 mW, the pulse duration increased from 2.75 to 4.1 ns, the narrowest pulse duration was 2.2 ns under a pump power of 79 mW. The value of pulse duration would decrease under the pump power above 226.4 mW. Because the nonlinear effect of the fiber would be improved under the high pump power. In the meantime, when the pump power rose from 44.8 to 319.7 mW, the output power increased was up-regulated 0.402–5.15 mW. Fig. 7(b) suggests that, the output power and the pulse duration acted as a function of pump power in a mode-locked fiber laser, which includes PD-ISO, SMF and SnS_2-PVA film. When pump power increased from 53.1 to 193.3 mW, the output power rose from 0.173 to 1.023 mW. The pulse duration was reduced from 1.7 to 1.05 ns, and the narrowed pulse duration was 1.05 ns under a pump power of 193.3 mW. The value of the pulse duration would increase under the pump power above 193.3 mW. By comparing the data in above graphs, the pulse duration is found compressed after added the SnS_2-PVA film. The pulse duration was shorted to one half or one third of the original. Cheng et al. have demonstrated reduce the length of the SMF can effectively decrease the pulse width, which attributed to the cavity dispersion is changed [41]. Therefore, in this study, the phenomenon of pulse duration shorted was also attributed to the change of cavity dispersion. Due to the length of the SMF not change, therefore, we concluded the phenomenon was attributed to the dispersion effect of the SnS_2-PVA film. To the best of our knowledge, this study initially investigated the dispersion characteristics of the SAs in all-normal-dispersion passively mode-locked Yb-doped fiber laser.

As shown in Fig. 8(a), the single pulse train of the mode-locked fiber laser without SA under the pump power of 319.7 mW was recorded, with the full width high maximum (FWHM) of 2.5 ns. The inset was multi-pulse train under the same pump power. Besides, in Fig. 8(b), the single pulse train of the mode-locked fiber laser with SA under the pump power of 214 mW was recorded, with the FWHM of 1.55 ns. The multi-pulse train was also recorded and shown in the inset of Fig. 8(b).

Besides, stability is one of the critical parameters of passively mode-locked fiber laser. To characterize the stability of the mode-locked fiber laser, a spectrum analyzer (R&S FPC1000) was employed to record the radio frequency spectrum. The radio frequency (RF) spectrum of the mode-locked fiber laser without SA was recorded, as shown in Fig. 9(a). The radio frequency spectrum located at a fundamental repetition rate of 677.6 kHz, with a bandwidth of 1400 kHz, a resolution of 300 Hz, and the single-to-noise ratio of 28 dB. The radio frequency spectrum within a wide bandwidth of 18 MHz is shown in the inset of Fig. 9(a). The radio frequency (RF) spectrum of the mode-locked fiber laser with SnS_2-PVA film was recorded, as shown in Fig. 9(b). The radio frequency spectrum located at a fundamental repetition rate of 675.1 kHz with a bandwidth of 1400 kHz and a resolution of 300 Hz, the single-to-noise ratio is 40 dB. The radio frequency spectrum within a wide bandwidth of 18 MHz is shown in the inset of Fig. 9(b). This study found that the single-to-noise ratio was improved after adding the SnS_2-PVA film, which implies that the stability of the mode-locked pulse was improved.

In Fig. 10(a), the typical dual-wavelength emission spectrum of the mode-locked fiber laser without SA was recorded using an optical spectrum analyzer (AQ-6317) under a resolution of 0.02 nm. An obvious dual-wave-length spectrum located at 1031.08 and 1034.19 nm was clearly observed. The emission spectrum of the mode-locked fiber laser with SnS_2-PVA film is shown in Fig. 10(b). The central wavelength and 3 dB bandwidth reached 1027.71 and 0.064 nm, respectively.

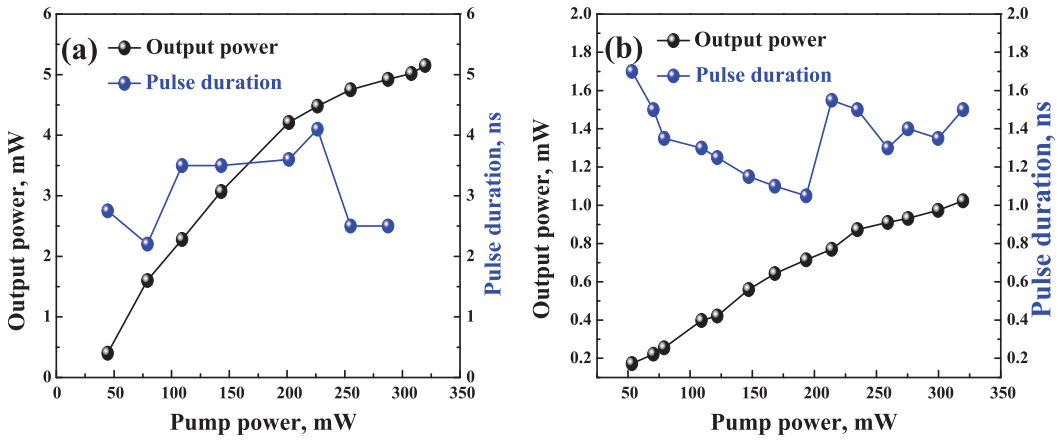

Fig. 7. (a) PD-ISO and SMF: The output power and the pulse duration as a function of pump power. (b) PD-ISO, SMF and SnS_2-PVA film: The output power and the pulse duration as a function of pump power.

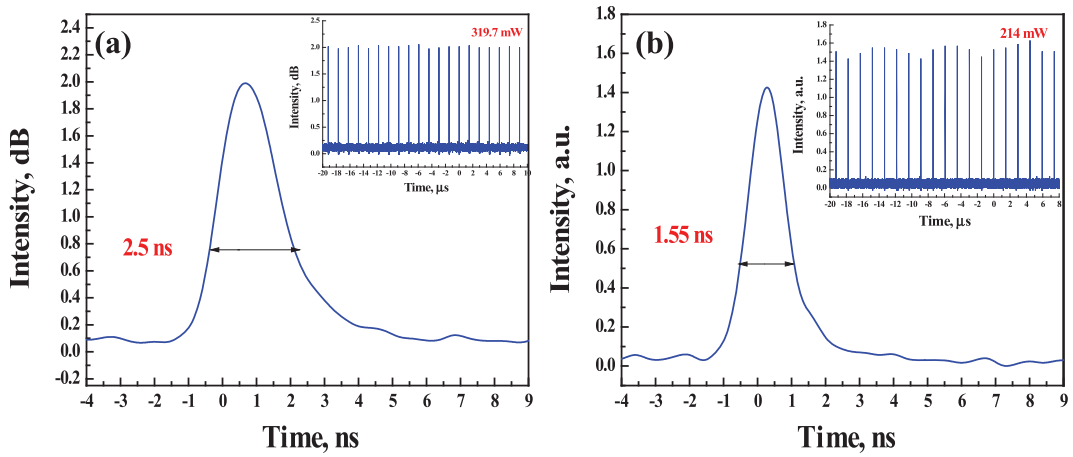

Fig. 8. (a) PD-ISO and SMF: single pulse train and multi-pulse train recorded with oscilloscope under the pump power of 319.7 mW; (b) PD-ISO, SMF and SnS_2-PVA film: single pulse train and multi-pulse train recorded with oscilloscope under the pump power of 214 mW.

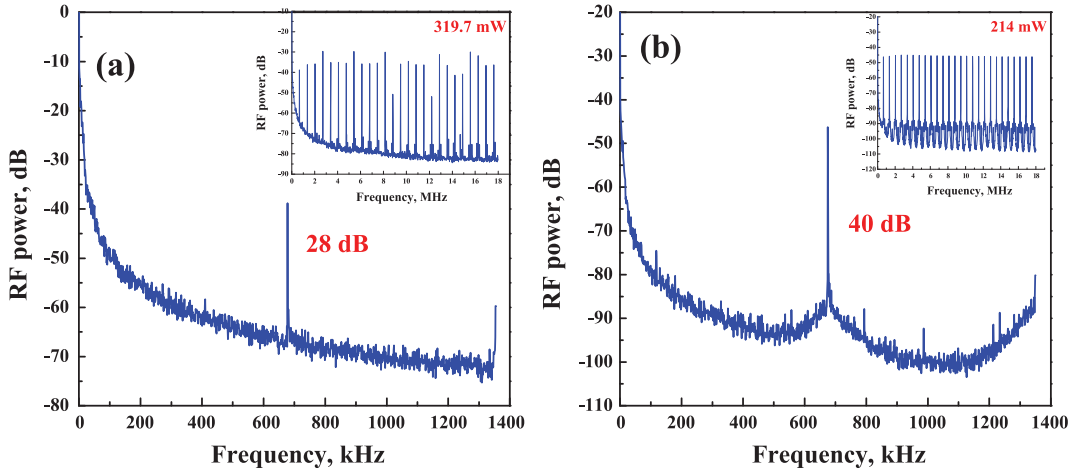

Fig. 9. (a) PD-ISO and SMF: RF spectrum of the mode-locked YDFL at pump power of 319.7 mW. Inset is RF spectrum with 18 MHz. (b) PD-ISO, SMF and SnS_2-PVA film: RF spectrum of the mode-locked YDFL at pump power of 214 mW. Inset is RF spectrum with 18 MHz.

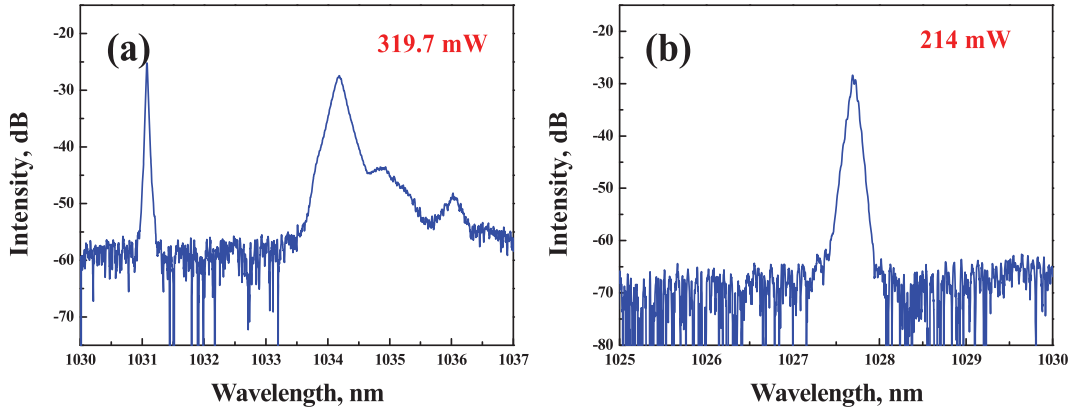

Fig. 10. (a) PD-ISO and SMF: Emission spectrum. (b) PD-ISO, SMF and SnS_2-PVA film: Emission spectrum.

5. Conclusion

To sum up, this study initially investigated the dispersion effect of the SnS_2-PVA film in an all-normal-dispersion passively mode-locked Yb-doped fiber laser. We found that the dispersion effect of SnS_2 nanosheets significantly decreased pulse width. By compressing, the narrowest pulse width was 1.05 ns under the pump power of 193.3 mW. The results here demonstrated that the dispersion effect of the SAs is worth investigating, which will facilitate the practical applications of SAs in ultrafast photonics.

Declaration of Competing Interest

There is no conflict of interest.

Acknowledgements

The authors acknowledge the support from the National Natural Science Foundation (NSFC) (Grant No. 11674199, 51707111, 61205174, 11474187), the Shandong Province Natural Science Foundation (2017GGX20120, ZR2016FP01) and the China Postdoctoral science Foundation (2016M602177).

References

[1] N. Nishizawa, Ultrashort pulse fiber lasers and their applications, Jpn. J. Appl. Phys. 53 (2014) 090101.
[2] K. Scholle, P. Fuhrberg, P. Koopmann, S. Lamrini, 2 μm laser sources and their possible applications, INTECH Open 82 (2010) 471–503.
[3] M.E. Fermann, I. Hartl, Ultrafast fiber lasers, Nat. Photon. 7 (2013) 868–874.
[4] B. Guo, 2D noncarbon materials-based nonlinear optical devices for ultrafast photonics, Chin. Opt. Lett. 16 (2018) 020004.
[5] P. Grelu, N. Akhmediev, Dissipative solitons for mode-locked lasers, Nat. Photon. 6 (2012) 84–92.
[6] B. Oktem, C. Ülgüdür, F.Ö. Ilday, Soliton–similariton fiber laser, Photonics 4 (2010) 307–311.
[7] W.H. Renninger, A. Chong, F.W. Wise, Pulse shaping and evolution in normal-dispersion mode-locked fiber lasers, IEEE J. Sel. Top. Quant. Electron. 18 (2012) 389–398.
[8] J. Liu, J. Xu, P. Wang, High repetition-rate narrow bandwidth SESAM mode-locked Yb-doped fiber lasers, IEEE Photon. Technol. Lett. 24 (2012) 539–541.
[9] P.X. Li, Z.Q. Zhao, M.M. Zhang, B.X. Liang, J.J. Chi, C. Yang, G.J. Zhang, H.W. Hu, Y.F. Yao, C.M. Ma, Subpicosecond SESAM and nonlinear polarization evolution hybrid mode-locking ytterbium-doped fiber oscillator, Appl. Phys. B: Lasers Opt. 118 (2015) 561–566.
[10] H. Zhang, D.Y. Tang, R.J. Knize, L.M. Zhao, Q.L. Bao, K.P. Loh, Graphene mode locked, wavelength-tunable, dissipative soliton fiber laser, Appl. Phys. Lett. 96 (2010) 111112.
[11] D. Popa, Z. Sun, F. Torrisi, T. Hasan, F. Wang, A.C. Ferrari, Sub 200 fs pulse generation from a graphene mode-locked fiber laser, Appl. Phys. Lett. 97 (2010) 203106.
[12] Z.P. Sun, T. Hasan, F. Torrisi, D. Popa, G. Privitera, F.Q. Wang, F. Bonaccorso, D.M. Basko, A.C. Ferrari, Graphene mode-locked ultrafast laser, ACS Nano 4 (2010) 803–810.
[13] Z.P. Sun, D. Popa, T. Hasan, F. Torrisi, F.Q. Wang, E.J.R. Kelleher, J.C. Travers, V. Nicolosi, A.C. Ferrari, A stable, wideband tunable, near transform-limited, graphene-mode-locked, ultrafast laser, Nano Res. 3 (2010) 653–660.
[14] F. Bonaccorso, Z. Sun, T. Hasan, A.C. Ferrari, Graphene photonics and optoelectronics, Nat. Photon. 4 (2010) 611–622.
[15] M.A. Solodyankin, E.D. Obraztsova, A.S. Lobach, A.I. Chernov, A.V. Tausenev, V.I. Konov, E.M. Dianov, Mode-locked 1.93 μm thulium fiber laser with a carbon nanotube absorber, Opt. Lett. 33 (2008) 1336–1338.
[16] F. Wang, A.G. Rozhin, V. Scardaci, Z. Sun, F. Hennrich, I.H. White, W.I. Milne, A.C. Ferrari, Wideband-tuneable, nanotube mode-locked, fibre laser, Nat. Nanotechnol. 3 (2008) 738–742.
[17] X. Zhao, Z. Zheng, L. Liu, Y. Liu, Y.X. Jiang, X. Yang, J.S. Zhu, Switchable, dual-wavelength passively mode-locked ultrafast fiber laser based on a single-wall carbon nanotube modelocker and intracavity loss tuning, Opt. Exp. 19 (2011) 1168–1173.
[18] N. Nishizawa, Y. Seno, K. Sumimura, Y. Sakakibara, E. Itoga, H. Kataura, K. Itoh, All-polarization-maintaining Er-doped ultrashort-pulse fiber laser using carbon nanotube saturable absorber, Opt. Exp. 16 (2008) 9429–9435.
[19] Z.C. Luo, M. Liu, H. Liu, X.W. Zheng, A.P. Luo, C.J. Zhao, H. Zhang, S.C. Wen, W.C. Xu, 2 GHz passively harmonic mode-locked fiber laser by a microfiber-based topological insulator saturable absorber, Opt. Lett. 38 (2013) 5212–5215.
[20] H. Liu, X.W. Zheng, M. Liu, N. Zhao, A.P. Luo, Z.C. Luo, W.C. Xu, H. Zhang, C.J. Zhao, S.C. Wen, Femtosecond pulse generation from a topological insulator mode-locked fiber laser, Opt. Exp. 22 (2014) 6868–6873.
[21] C.J. Zhao, Y.H. Zou, Y. Chen, Z.T. Wang, S.B. Lu, H. Zhang, S.C. Wen, D.Y. Tang, Wavelength-tunable picosecond soliton fiber laser with topological insulator: Bi_2Se_3 as a mode locker, Opt. Exp. 20 (2012) 27888–27895.
[22] Y.H. Lin, C.Y. Yang, S.F. Lin, W.H. Tseng, Q.L. Bao, C.I. Wu, G.R. Lin, Soliton compression of the erbium-doped fiber laser weakly started mode-locking by nanoscale p-type Bi_2Te_3 topological insulator particles, Laser Phys. Lett. 11 (2014) 055107.
[23] J. Sotor, G. Sobon, W. Macherzynski, K.M. Abramski, Harmonically mode-locked Er-doped fiber laser based on a Sb_2Te_3 topological insulator saturable absorber, Laser Phys. Lett. 11 (2014) 055102.
[24] Y. Zhou, Q. Miao, Y.P. Sun, F. Gel'mukhanov, C.K. Wang, Solvent effect on dynamical TPA and optical limiting of BDMAS molecular media for nanosecond and femtosecond laser pulses, J. Phys. B: At., Mol. Opt. Phys. 44 (2011) 035103.
[25] N.N. Xu, N. Ming, X.L. Han, B.Y. Man, H.N. Zhang, Large-energy passively Q-switched Er-doped fiber laser based on CVD-Bi_2Se_3 as saturable absorber, Opt. Mater. Exp. 9 (2019) 373–383.
[26] H.D. Xia, H.P. Li, C.Y. Lan, C. Li, X.X. Zhang, S.J. Zhang, Y. Liu, Ultrafast erbium-doped fiber laser mode-locked by a CVD-grown molybdenum disulfide (MoS_2) saturable absorber, Opt. Exp. 22 (2014) 17341–17348.
[27] J. Du, Q.K. Wang, G.B. Jiang, C.W. Xu, C.J. Zhao, Y.J. Xiang, Y. Chen, S.C. Wen, H. Zhang, Ytterbium-doped fiber laser passively mode locked by few-layer molybdenum disulfide (MoS_2) saturable absorber functioned with evanescent field interaction, Sci. Rep. 4 (2014) 6346.
[28] D. Mao, Y.D. Wang, C.J. Ma, L. Han, B.Q. Jiang, X.T. Gan, S.J. Hua, W.D. Zhang, T. Mei, J.L. Zhao, WS_2 mode-locked ultrafast fiber laser, Sci. Rep. 5 (2015) 7965.
[29] P.G. Yan, A.J. Liu, Y.S. Chen, J.Z. Wang, S.C. Ruan, H. Chen, J.F. Ding, Passively mode-locked fiber laser by a cell-type WS_2 nanosheets saturable absorber, Sci. Rep. 5 (2015) 12587.
[30] B.H. Chen, X.Y. Zhang, K. Wu, H. Wang, J. Wang, J.P. Chen, Q-switched fiber laser based on transition metal dichalcogenides MoS_2, $MoSe_2$, WS_2, and WSe_2, Opt. Exp. 23 (2015) 26723–26737.
[31] D. Mao, X.Y. She, B.B. Du, D.X. Yang, W.D. Zhang, K. Song, X.Q. Cui, B.Q. Jiang, T. Peng, J.L. Zhao, Erbium-doped fiber laser passively mode locked with few-layer $WSe_2/MoSe_2$ nanosheets, Sci. Rep. 6 (2016) 23583.
[32] N. Ming, S.N. Tao, W.Q. Yang, Q.Y. Chen, R.Y. Sun, C. Wang, S.Y. Wang, B.Y. Man, H.N. Zhang, Mode-locked Er-doped fiber laser based on PbS/CdS core/shell quantum dots as saturable absorber, Opt. Exp. 26 (2018) 9017–9026.
[33] N.N. Xu, H.N. Zhang, W.Q. Yang, X.L. Han, B.Y. Man, High-efficiency passively Q-switched neodymium-doped fiber laser operation at 1360.61 nm with bismuth selenide as saturable absorber, Laser Phys. 28 (2018) 125801.
[34] Y.Q. Ge, Z.F. Zhu, Y.H. Xu, Y.X. Chen, S. Chen, Z.M. Liang, Y.F. Song, Y.S. Zou, H.B. Zeng, S.X. Xu, H. Zhang, D.Y. Fan, Broadband nonlinear photoresponse of 2D TiS_2 for ultrashort pulse generation and all-optical thresholding devices, Adv. Opt. Mater. 6 (2018) 1701166.
[35] X.T. Jiang, S.X. Liu, W.Y. Liang, S.J. Luo, Z.L. He, Y.Q. Ge, H.D. Wang, R. Cao, F. Zhang, Q. Wen, J.Q. Li, Q.L. Bao, D.Y. Fan, H. Zhang, Broadband nonlinear photonics in few-layer MXene Ti_3C_2Tx (T = F, O, or OH), Laser Photon. Rev. 12 (2018) 1700229.
[36] W.N. Ren, H.F. Zhang, C. Guan, C.W. Cheng, Ultrathin MoS_2 nanosheets@ metal organic framework-derived n-doped carbon nanowall arrays as sodium ion battery anode with superior cycling life and rate capability, Adv. Funct. Mater. 27 (2017) 1702116.
[37] J. Sotor, G. Sobon, M. Kowalczyk, W. Macherzynski, P. Paletko, K.M. Abramski, Ultrafast thulium-doped fiber laser mode locked with black phosphorus, Opt. Lett. 40 (2015) 3885–3888.
[38] Z.C. Luo, M. Liu, Z.N. Guo, X.F. Jiang, A.P. Luo, C.J. Zhao, X.F. Yu, W.C. Xu, H. Zhang, Microfiber-based few-layer black phosphorus saturable absorber for ultra-fast fiber laser, Opt. Exp. 23 (2015) 20030–20039.
[39] Y. Chen, G.B. Jiang, S.Q. Chen, Z.N. Guo, X.F. Yu, C.J. Zhao, H. Zhang, Q.L. Bao, S.C. Wen, D.Y. Tang, D.Y. Fan, Mechanically exfoliated black phosphorus as a new saturable absorber for both Q-switching and mode-locking laser operation, Opt. Exp. 23 (2015) 12823–12833.
[40] B. Guo, S.H. Wang, Z.X. Wu, Z.X. Wang, D.H. Wang, H. Huang, F. Zhang, Y.Q. Ge, H. Zhang, Sub-200 fs soliton mode-locked fiber laser based on bismuthene saturable absorber, Opt. Exp. 26 (2018) 22750–22760.
[41] D. Mao, X.Q. Cui, X.T. Gan, M.K. Li, W.D. Zhang, H. Lu, J.L. Zhao, Passively Q-switched and mode-locked fiber laser based on a ReS_2 saturable absorber, IEEE J. Sel. Top. Quant. Electron. 24 (2018) 1100406.
[42] K.D. Niu, Q.Y. Chen, R.Y. Sun, B.Y. Man, H.N. Zhang, Passively Q-switched erbium-doped fiber laser based on SnS_2 saturable absorber, Opt. Mater. Exp. 7 (2017) 3934–3943.
[43] K.D. Niu, R.Y. Sun, Q.Y. Chen, B.Y. Man, H.N. Zhang, Passively mode-locked Er-doped fiber laser based on SnS_2 nanosheets as a saturable absorber, Photon. Res. 6 (2018) 72–76.
[44] J.H. Lin, C.W. Chan, H.Y. Lee, Y.H. Chen, Bound states of dispersion-managed solitons from single-mode Yb-doped fiber laser at net-normal dispersion, IEEE Photon. J. 7 (2015) 1–9.
[45] Z.C. Cheng, S.D. Wu, H.X. Shi, J. Xu, Q.H. Yang, P. Wang, Dissipative soliton resonance in an all-normal-dispersion graphene oxide mode-locked Yb-doped fiber laser, in: CLEO: Science and Innovations CM1I-6, 2013, pp. 1–2.
[46] J.W. Seo, J.T. Jang, S.W. Park, C.J. Kim, B.W. Park, J.W. Cheon, Two-dimensional SnS_2 nanoplates with extraordinary high discharge capacity for lithium ion batteries, Adv. Mater. 5 (2008) 5226–5230.
[47] B. Luo, Y. Fang, B. Wang, J.S. Zhou, H.H. Song, L.J. Zhi, Two dimensional graphene-SnS_2 hybrids with superior rate capability for lithium ion storage, Energy Environ. Sci. 5 (2012) 5226–5230.
[48] J.T. Zai, K.X. Wang, Y.Z. Su, X.F. Qian, J.S. Chen, High stability and superior rate capability of three-dimensional hierarchical SnS_2 microspheres as anode material in lithium ion batteries, J. Power Sources 196 (2011) 3650–3654.
[49] A.J. Smith, P.E. Meek, W.Y. Liang, Raman scattering studies of SnS_2 and $SnSe_2$, J. Phys. C 10 (1977) 1321–1323.
[50] W.Q. Yang, N.N. Xu, H.N. Zhang, Nonlinear absorption properties of indium selenide and its application for demonstrating pulsed Er-doped fiber laser, Laser Phys. Lett. 15 (2018) 105101.
[51] J.H. Ahn, M.J. Lee, H. Heo, J.H. Sung, K. Kim, H. Hwang, M.H. Jo, Deterministic two-dimensional polymorphism growth of hexagonal n-type SnS_2 and orthorhombic p-type SnS crystals, Nano Lett. 15 (2015) 3703–3708.
[52] B. Guo, Q. Lyu, Y. Yao, P.F. Wang, Direct generation of dip-type sidebands from WS_2 mode-locked fiber laser, Opt. Mater. Exp. 6 (2016) 2475–2486.